Acta Crystallographica Section D
Biological Crystallography
ISSN 0907-4449

Pseudo-merohedral twinning in crystals of the dihaem *c*-type cytochrome DHC2 from *Geobacter sulfurreducens*

Daniel Heitmann and Oliver Einsle*

Institut für Mikrobiologie und Genetik, Abteilung Molekulare Strukturbiologie, Georg-August-Universität Göttingen, Justus-von-Liebig-Weg 11, 37077 Göttingen, Germany

Correspondence e-mail: oeinsle@uni-goettingen.de

Received 31 March 2008
Accepted 24 June 2008

The dihaem cytochrome DHC2 from *Geobacter sulfurreducens* has been described as a model system for the study of one of the conserved haem-packing motifs typically observed in multihaem cytochromes *c*, in which the covalent attachment of haem to the protein allows effective spatial clustering of redox centres and a high haem:protein ratio. Heterologously expressed DHC2 has been crystallized previously and the structure has been solved by multiple-wavelength anomalous dispersion (MAD) and refined to a resolution of 1.5 Å (PDB code 2czs). Crystals belonged to the monoclinic space group $P2_1$, with unit-cell parameters a = 39.65, b = 55.68, c = 39.64 Å, β = 105.91°. Close inspection of the data indicated the presence of pseudo-merohedral twinning; while not hindering structure solution by MAD, this resulted in high refinement R factors. A re-assessment of the diffraction data for DHC2 is presented, together with a refined structure that includes the twinning present with a twinning fraction α of 0.32.

1. Introduction

Haem-containing cytochromes are essential parts of the electron-transport chains of aerobic respiration and photosynthesis in eukaryotic organisms, as well as in the majority of anaerobic respiratory pathways in prokaryotes (Gouterman, 1978). Cytochromes of the *c* type are characterized by the covalent attachment of the haem group to the protein chain *via* two thioether bonds from the cysteines of a conserved C*XX*CH binding motif to the vinyl side chains of the porphyrin moiety (Thöny-Meyer, 1997). These bonds are formed by one of several known types of cytochrome *c* maturation system localized in the cytoplasmic membrane. Covalent bonding of the cofactor supports protein stability and allows the tight packing of what may be very large numbers of haem groups (Stevens *et al.*, 2004; Barker & Ferguson, 1999). Strikingly, structural analyses of multihaem cytochromes revealed the conservation of haem–haem interaction motifs rather than of protein sequence or structure. In particular, parallel and perpendicular haem-packing motifs with unknown biochemical functions have been identified (Iverson *et al.*, 1998; Einsle *et al.*, 2000; Einsle, 2001).

DHC2, an 11.3 kDa dihaem *c*-type cytochrome from the ε-proteobacterium *Geobacter sulfurreducens*, was recombinantly expressed in *Escherichia coli* and characterized biochemically as well as by X-ray crystallography (Heitmann & Einsle, 2005). Its two haem groups form the conserved parallel haem-packing motif that has previously been observed in complex redox proteins such as hydroxylamine oxidoreductase from *Nitrosomonas europaea* (Igarashi *et al.*, 1997) and cytochrome *c* nitrite reductase from *Sulfurospirillum deleyianum* (Einsle *et al.*, 1999) and *Wolinella succinogenes* (Einsle *et al.*, 2000). Spectroscopic studies on these large multihaem proteins are often complicated by the sheer number and strong electronic interactions of the haem cofactors. In order to understand the properties of the recurring haem-interaction motifs it therefore seemed imperative to identify systems of lower complexity that nevertheless retain the structural properties of the packing motifs found in the large oxidoreductases. DHC2 was chosen from more than 100 genes coding for *c*-type cytochromes in the genome of the metal-reducing soil bacterium *G. sulfurreducens*. It represents a

Table 1
Data-integration and structure-refinement statistics of DHC2.

Values in parentheses are for the highest resolution shell.

Data collection			
Wavelength (Å)	0.994		
Resolution range (Å)	50.0–1.5 (1.52–1.50)		
Merging			
Space group	$C222_1$	$P2_1$	
R_{merge}†	0.17 (0.59)	0.05 (0.56)	
$R_{r.i.m.}$‡	0.18 (0.64)	0.06 (0.62)	
$R_{p.i.m.}$§	0.05 (0.24)	0.02 (0.31)	
Refinement			
Twinning operation¶	N/A	$l, -k, h$	
Resolution range (Å)	N/A	50.0–1.5	
Refined twin fraction	N/A	0.322	
		Untwinned	Twinned
R_{cryst}††	N/A	0.223	0.176
R_{free}††	N/A	0.278	0.227
R.m.s.d. from ideality‡‡			
Bond lengths (Å)	N/A	0.008	0.009
Bond angles (°)	N/A	2.2	2.3
Ramachandran plot‡‡			
Core (%)	N/A	89.2	89.2
Allowed (%)	N/A	10.8	10.8
Disallowed (%)	N/A	0	0

† R_{merge} is the merging R factor; $R_{merge} = \sum_{hkl}\sum_i |I_i(hkl) - \langle I(hkl)\rangle| / \sum_{hkl}\sum_i I_i(hkl)$. ‡ $R_{r.i.m.}$ is the redundancy-independent merging R factor (Weiss & Hilgenfeld, 1997); $R_{r.i.m.} = \sum_{hkl}[N/(N-1)]^{1/2}\sum_i |I_i(hkl) - \langle I(hkl)\rangle| / \sum_{hkl}\sum_i I_i(hkl)$. § $R_{p.i.m.}$ is the precision-indicating merging R factor (Weiss & Hilgenfeld, 1997); $R_{p.i.m.} = \sum_{hkl}[1/(N-1)]^{1/2}\sum_i |I_i(hkl) - \langle I(hkl)\rangle| / \sum_{hkl}\sum_i I_i(hkl)$. ¶ The twin operation corresponds to the twin law relating individual twin domains by a fractional ratio given by the refined twin fraction *(SHELXL*; Sheldrick, 2008). †† The refinement R factor $R_{cryst} = \sum_{hkl} ||F_{obs}(hkl)| - k|F_{calc}(hkl)|| / |F_{obs}(hkl)|$; R_{free} includes 5% of the test-set reflections. ‡‡ The The r.m.s.d. from ideality and Ramachandran plot were calculated using *PROCHECK* (Laskowski *et al.*, 1993).

straightforward and versatile model system of low complexity that allows spectroscopic and structural studies of a single parallel haem-packing motif and is easily accessible for site-directed mutagenesis studies (Heitmann & Einsle, 2005). However, at the current resolution of 1.5 Å refinement of the structure of DHC2 did not proceed beyond R_{cryst} = 0.221 and R_{free} = 0.272, pointing towards possible problems that we now address in a re-evaluation of the diffraction data. Indicators for crystal twinning were found and will be discussed in further detail in the following.

Crystal twinning denotes the presence of two or more individuals within a macroscopic crystalline body. These can be distinct intergrown single crystals, leading to separate overlapping diffraction patterns. In the more complex case of merohedral twinning the individuals are not required to occupy distinct areas within the crystal and their mutual orientation is specific, leading to changes in reflection intensity (Friedel, 1926; Giacovazzo, 1992; Yeates, 1997; Parsons, 2003). Individuals are related by a spatial transformation (twinning) operation and a twin fraction α, the ratio in which individual twin domains contribute to the overall intensity of diffraction maxima (Herbst-Irmer & Sheldrick, 1998). Merohedrally twinned crystals include symmetry elements that are not part of the true Laue group of the crystal, but of a holohedral point group of the same crystal system, limiting their occurrence to the tetragonal, trigonal, hexagonal and cubic crystal systems. The lattices of twin-related domains coincide perfectly, so that this type of twinning can only be detected through inspection of intensity statistics (Liang *et al.*, 1996; Yeates & Fam, 1999; Dauter, 2003).

In the case of pseudo-merohedral twinning, the twinning operation is not a symmetry operation of a holohedral point group of specialized metric, but of an apparently higher crystal system approximately corresponding to the present crystal metric. The better the reciprocal-space lattices approximate the higher metric symmetry, the less evidence for twinning can be drawn from inspection of the diffraction pattern. The twinning operation in this case is an element of the apparent higher symmetry but not of the correct symmetry class of the crystal. The difference between these two crystal classes can become apparent in high-resolution diffraction spots (Herbst-Irmer & Sheldrick, 1998).

In monoclinic crystal systems, pseudo-merohedral twinning can occur if the unit-cell parameters allow approximate restoration of the lattice by the twin operation, *i.e.* different orientations of the cell within the crystal lattice. This condition can be met in several ways. For instance, an angle β of or close to 90° conveys an orthorhombic appearance to a primitive monoclinic unit cell and will add to the crystallographic twofold defined by the monoclinic operation $-h, k, -l$ the possibility of twofold rotations around the basis vectors **a** or **c**. The result is pseudo-merohedral twinning with the (noncrystallographic) twinning operations $h, -k, -l$ or $-h, -k, l$, respectively (Larsen *et al.*, 2002). A second possibility for twinning requires that the unit-cell parameters fulfil the condition $c\cos\beta = -a/2$ and the twinning operation is a rotation around **c***, the vector normal to the **ab** (001) plane. The twin domains thus share the same **a** and **b**, albeit with opposite signs. The data can be indexed as *C*-centred orthorhombic and the corresponding twinning operation is $-h, -k, h + 1$ (Declercq & Evrard, 2001; Rudolph *et al.*, 2004). A third case of twinning in monoclinic systems requires **a** and **c** to be of equal length, allowing a rotation around the diagonal of the **ac** (010) plane. Again, this transformation appears as a *C*-centred orthorhombic system, now with a twinning operation $l, -k, h$ (Yang *et al.*, 2000; Wittmann & Rudolph, 2007; Sultana *et al.*, 2007).

2. Materials and methods

2.1. Structure solution by MAD

The production, crystallization and structure solution of DHC2 were carried out as described previously (Heitmann & Einsle, 2005). In brief, DHC2 from *G. sulfurreducens* was overproduced in *Escherichia coli* using the accessory plasmid pEC86 to allow the maturation of *c*-type cytochromes during aerobic expression of protein (Arslan *et al.*, 1998). The structure of DHC2 was solved by a multiple-wavelength anomalous dispersion (MAD) experiment using Fe *K*-edge data collected at three distinct wavelengths and refined to a resolution of 1.5 Å.

Data were indexed and integrated using the *HKL* suite (Otwinowski & Minor, 1997). Indexing was possible both with a primitive monoclinic Bravais lattice with unit-cell parameters a = 39.64, b = 55.67, c = 39.63 Å, β = 105.91° and with a *C*-centred orthorhombic system with unit-cell parameters a = 47.76, b = 63.27, c = 55.67 Å. Structure determination using the peak and inflection data was not possible in the *C*-centred orthorhombic cell, but a clear solution could be obtained in space group $P2_1$. Four Fe atoms per asymmetric unit were located with *SHELXD* (Schneider & Sheldrick, 2002) and phase calculations and further electron-density improvement were carried out using *SHELXE* (Sheldrick, 2002). The final model comprised two monomers of DHC2 in the asymmetric unit, with a total of 137 amino acids and four haem groups (Matthews coefficient of 1.87 Å^3 Da^{-1} and 34.3% solvent content; Matthews, 1968). Refinement was carried out in *REFMAC* (Murshudov *et al.*, 1997), resulting in a final crystallographic R factor of 0.221 and an R_{free} of 0.272 (Brünger, 1993).

3. Results and discussion

3.1. Indicators for pseudo-merohedral twinning in DHC2 crystals

The initial refinement of DHC2 in space group $P2_1$ resulted in conspicuously high refinement R factors for the obtained resolution

of 1.5 Å. Together with the *a* and *c* cell axes being equal in length, a telltale sign of possible pseudo-merohedral twinning, this finding prompted a detailed analysis of twinning indicators, with the aim of a better correlation between experimental data and structural model. DHC2 contained two monomers per asymmetric unit of the $P2_1$ cell and with $a \simeq c$ data processing was also possible in the orthorhombic space group $C222_1$, yielding a unit cell of exactly double the volume (168 962 Å^3). Inspection of unmerged diffraction data from *SCALEPACK* (Otwinowski & Minor, 1997) with the program *RMERGE* (Weiss, 2001) revealed a high merging *R* factor of 0.17 for the $C222_1$ cell compared with only 0.05 for the $P2_1$ cell. The redundancy-independent merging factor $R_{\rm r.i.m.}$ (Weiss & Hilgenfeld, 1997), with values of 0.06 for the $P2_1$ cell and 0.18 for the $C222_1$ cell, also clearly favoured $P2_1$ as the correct choice of space group (Table 1). Additionally, the precision-indicating *R* factor $R_{\rm p.i.m.}$ (Weiss & Hilgenfeld, 1997) for data scaled in $C222_1$ is twice that for $P2_1$ (0.02).

A further indication for twinning in DHC2 crystals was found in the $|E^2 - 1|$ value of 0.678 for acentric reflections, which lies significantly below the expected value of 0.736 (Herbst-Irmer & Sheldrick, 1998; Adams *et al.*, 2002). The normalized cumulative intensity distribution of $Z = I/\langle I\rangle$ calculated with a 2.0 Å resolution cutoff clearly differs from that for untwinned data for acentric reflections (Fig. 1*a*; Rees, 1980). The second moments of the normalized intensity distribution, $\langle I^2\rangle/\langle I\rangle^2$, and the analogous ratio of amplitudes, $\langle F^2\rangle/\langle F\rangle^2$, representing a twin-law-independent test for twinning, were examined using *CNS* (Brünger *et al.*, 1998). For untwinned data the ratio of intensities should be 2.0, decreasing to 1.5 for perfectly twinned data, with 0.785 and 0.865 for the ratio of amplitudes, respectively. In the case of DHC2 the observed ratios of 1.84 for intensities and 0.82 for amplitudes suggest the presence of crystal twinning with a fraction of $0 < \alpha < 0.5$ (Table 2).

In order to judge intensity statistics that were independent of effects such as anisotropic diffraction or pseudo-centring, the *L*-test was applied (Padilla & Yeates, 2003). It analyzes local intensity differences of reflections that lie close in reciprocal space and is

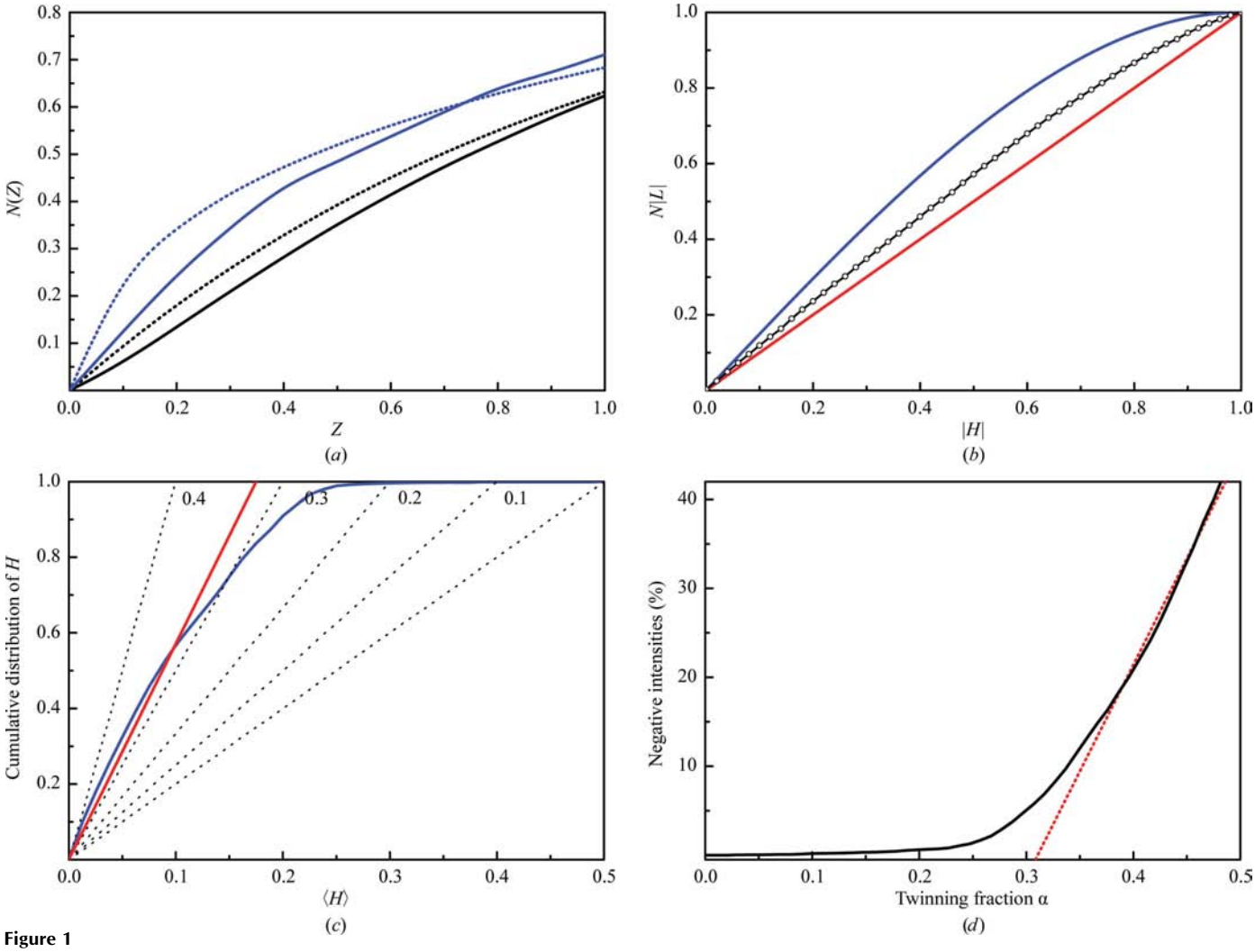

Figure 1
Analysis of intensity statistics and twin-fraction estimates in the process of twinning detection. (*a*) Cumulative distribution of $Z = I/\langle I\rangle$ for observed acentric reflections (black line) and centric reflections (blue line) of DHC2, calculated with data to 2.0 Å resolution. The theoretical distributions of untwinned data for acentric and centric reflections are shown as black and blue dotted lines, respectively. The sigmoidal shape of the observed acentric data indicates twinning. (*b*) The distribution of local statistics $L = I_1 - I_2/(I_1 + I_2)$, where I_1 and I_2 represent the intensities of unrelated reflections, is a test for the detection of twinning (*L*-test). The continuous red line represents the theoretical distribution of *L* for untwinned data and the continuous blue line that for a perfect twin. The observed distribution of *L* (black line) clearly differs from untwinned data. (*c*) Plot of the cumulative distribution of *H* for acentric reflections, with $H = |I_1 - I_2|/(I_1 + I_2)$ and intensities of reflections related by the twin law *l*, −*k*, *h* (*H*-test). Comparison of the observed distribution (blue line, with linear regression in red) with theoretical distributions of *H*, with a twin fraction increment of 0.1, yields a twin fraction $\alpha \simeq 0.33$. (*d*) Twin-fraction estimation by the Britton plot. Extrapolation of negative intensities against potential twin fraction α (black line) yields a twin fraction of $\alpha \simeq 0.31$ (red).

Table 2
Statistics of acentric data intensities for DHC2.

		Theoretical	
	Observed	Untwinned	Perfect twin
Wilson ratio and moments			
$\langle I^2\rangle/\langle I\rangle^2$	1.840	2.000	1.500
$\langle F^2\rangle/\langle F\rangle^2$	0.820	0.785	0.885
$\lvert E^2 - 1\rvert$	0.678	0.736	0.541
Yeates statistics†			
$\langle H\rangle$	0.169	0.50	0.0
$\langle H^2\rangle$	0.045	0.33	0.0
Padilla and Yeates statistics‡			
$\langle\lvert L\rvert\rangle$	0.449	0.500	0.375
$\langle L^2\rangle$	0.276	0.333	0.200

† According to Yeates (1997). ‡ According to Padilla & Yeates (2003).

implemented in the program *phenix.xtriage* (Adams *et al.*, 2002). The distribution of $|L|$ for DHC2 diffraction data again falls between the theoretical distributions for untwinned and perfectly twinned data (Fig. 1*b*). While clearly pointing towards pseudo-merohedral twinning in DHC2 crystals, the above tests were not suited to estimation of the twinning fraction α. Such information can be obtained from twin-law-dependent analyses such as the *H*-test (Yeates, 1997) and the Britton plot (Britton, 1972), as implemented in the program *DETWIN* (Collaborative Computational Project, Number 4, 1994). The *H*-test compares the cumulative distribution of *H*, with $H = |I_{\rm obs1} - I_{\rm obs2}|/(I_{\rm obs1} + I_{\rm obs2})$, and allows an estimate of the twinning fraction α by comparison with theoretical distributions of twinning fractions. To calculate *H*, a twinning axis in the **ac** (010) plane was assumed perpendicular to the crystallographic twofold along **b** and resulting in a twinning operation l, $-k$, h. A plot of *H* for DHC2 yielded an estimated twin fraction α of 0.33 (Fig. 1*c*). The Britton plot represents the number of negative intensities of measured data after detwinning. It should be zero while α is underestimated and change to a linear increase when it is overestimated. Extrapolation of the linearly increasing branch thus provides an estimate for α in the observed data, but also requires knowledge of the twinning operation relating the individual twin domains in order to perform detwinning. For DHC2, the Britton plot yielded a twinning fraction α of 0.31 (Fig. 1*d*).

The diffraction data were further examined for elements of noncrystallographic symmetry that form the structural basis of twinning. Calculation of a self-rotation function in space group $P2_1$ using the program *GLRF* (Tong & Rossmann, 1990) for $\kappa = 180^\circ$ revealed two maxima orthogonal to **b** with $\varphi = 0^\circ$, $\psi = -53^\circ$ and $\varphi = 0^\circ$, $\psi = 37^\circ$ sharing a relative height of 77.4% of the origin peak (Fig. 2). These peaks represent noncrystallographic symmetry axes parallel and perpendicular to the diagonal of the **ac** (010) plane, emulating a higher symmetry that allows indexing of the diffraction data in the *C*-centred orthorhombic space group $C222_1$.

Taken together, the statistical analyses presented above clearly point towards pseudo-merohedral twinning with a two to one ratio of the individual twin domains ($\alpha \simeq 0.33$). The twinning operation is a

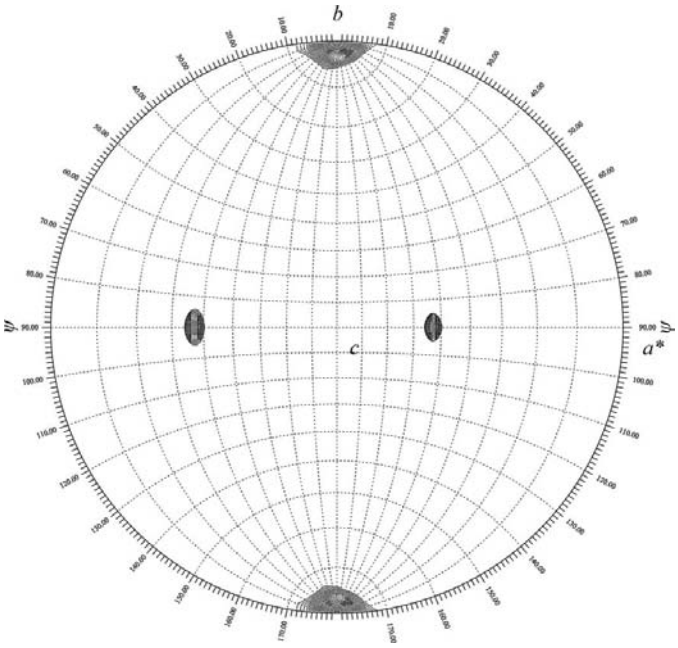

Figure 2
Self-rotation function depicting the noncrystallographic symmetry perpendicular to **b** in crystals of DHC2. The plot was generated with $\kappa = 180^\circ$ and reveals two prominent peaks perpendicular to **b**, with $\varphi = 0^\circ$, $\psi = -53.0^\circ$ and $\varphi = 0^\circ$, $\psi = 37.0^\circ$, at a height of 77.4% of the origin peak. The peaks are related to each other by a 90° rotation around **b**.

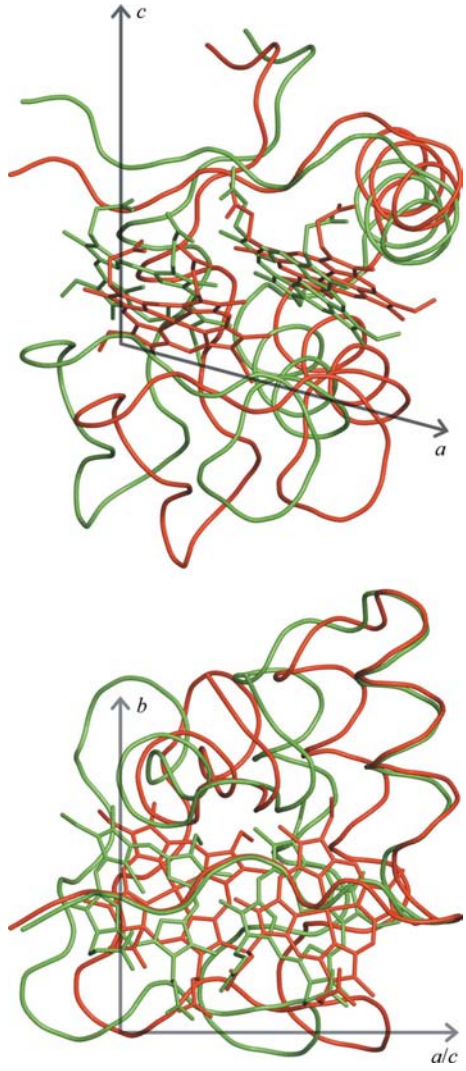

Figure 3
Superposition of $P2_1$ DHC2 monomer (red) in ribbon representation and the corresponding $C222_1$ symmetry monomer, created by combination of the idealized NCS operation $(-z + \frac{1}{2}, -y, -x + \frac{1}{2})$ with the second monomer in the asymmetric unit. The r.m.s.d. of 3.14 Å is a direct indication of the discrepancy of apparent pseudo-symmetry from higher symmetry.

rotation around the diagonal of the **ac** plane of the $P2_1$ cell, with the corresponding twinning operation being l, $-k$, h.

3.2. Twin refinement

For refinement against twinned data, 5% of the reflections were marked as test-set reflections using *CNS* to flag reflections according to the operation l, $-k$, h in order to avoid the simultaneous appearance of twin-related reflections in the test and working sets. This was performed to prevent twinning bias in the calculation of $R_{\rm free}$; in order to avoid another possible source of bias in $R_{\rm free}$ caused by a model that had previously been refined against a different working set, all further steps were started from the initial model of DHC2 built into an electron-density map calculated with *SHELXE* and never refined against diffraction data. *SHELXL* was used for refinement against twinned data and optimization of the twin fraction α (Sheldrick, 2008). After an initial round of rigid-body refinement in space group $P2_1$ with two monomers in the asymmetric unit, waters were included and a restrained refinement was performed that did not account for twinning. This resulted in an $R_{\rm cryst}$ of 0.223 and an $R_{\rm free}$ of 0.278, which were well in accordance with the refinement statistics obtained from *REFMAC*5 (Heitmann & Einsle, 2005). By including TWIN 0 0 1 0 −1 0 1 0 0 and BASF 0.1 (as starting value for the twinning fraction) into the refinement process, the R factors dropped by about 4.5% to final values of $R_{\rm cryst}$ of 0.176 and $R_{\rm free}$ of 0.227. The refined twin fraction of 0.322 corresponds to the values estimated by the H-test and the Britton plot. The model integrity of the twin-refined DHC2 structure was assured by *PROCHECK* (Laskowski *et al.*, 1993). The Ramachandran plot shows no difference for both models; the r.m.s.d. of bond lengths differs by 0.001 Å and that for bond angles by about 0.1°. The protein backbone shows an r.m.s.d. of 0.15 Å in atom positions, meaning that the structural model was essentially correct even when twinning was not taken into account.

3.3. Analysis of twinning

The two peaks observed in the self-rotation function of DHC2 (Fig. 2) indicate the presence of (i) a noncrystallographic symmetry axis orthogonal to **b**, relating the two monomers of the protein in the asymmetric unit, and (ii) a third twofold axis generated by the orthogonality of **b** and the NCS axis, leading to an apparent orthorhombic point-group symmetry. The superimposition of the two DHC2 monomers using *Coot* (Emsley & Cowtan, 2004; Krissinel & Henrick, 2004) yields an NCS operation (in fractional coordinates) of

$$R = \begin{pmatrix} -0.22 & 0.006 & -0.994 \\ 0.014 & -1.000 & -0.008 \\ -1.006 & -0.027 & 0.022 \end{pmatrix}, \quad T = \begin{pmatrix} 0.46 \\ -0.03 \\ 0.54 \end{pmatrix}.$$

This operation just barely misses the ideal $(-z+\frac{1}{2}, -y, -x+\frac{1}{2})$ which, together with the orthogonal operations $(z+\frac{1}{2}, -y+\frac{1}{2}, x+\frac{1}{2})$, would result in the symmetry operations of a C-centred orthorhombic lattice with space group $C222_1$. A superimposition of coordinates for a $C222_1$ symmetry-idealized monomer of DHC2 with the related pseudo-symmetry equivalent (Fig. 3) calculated with the program *PDBSET* (Collaborative Computational Project, Number 4, 1994) has a root-mean-squared deviation of 3.14 Å, indicating the discrepancy between 'real' higher symmetry and pseudo-symmetry. Any primitive monoclinic lattice with $a \simeq c$ can accommodate a C-centred orthorhombic cell with unit-cell axes $a' = 2a\cos(\beta/2)$, $b' = 2a\sin(\beta/2)$ and $c' = b$ (Fig. 4*a*), but the occurrence of pseudo-merohedry requires the presence of additional symmetry operations that almost (but not quite) fulfil the requirements of $C222_1$. In DHC2 crystals, the packing of molecules in the $P2_1$ cell necessitates an origin shift of $(\frac{1}{4}, \frac{1}{4}, \frac{1}{4})$ in order to make the NCS axes coincide with the crystallographic axes of the $C222_1$ cell. In this setup, the divergence between the actual NCS operations in DHC2 and those of the higher symmetry space group that in effect allows twinning by pseudo-merohedry is clearly visible (Figs. 4*b* and 4*c*). The symmetry elements then appear as twinning operations in the lower symmetry monoclinic crystal system and the resulting twin law is l, $-k$, h. The existence of NCS approximately parallel to the apparent twin axis leads to intensity statistics that are different from pathological twinning cases, as reflections related by twinning gain an additional relation through the approximately parallel NCS axis. This becomes

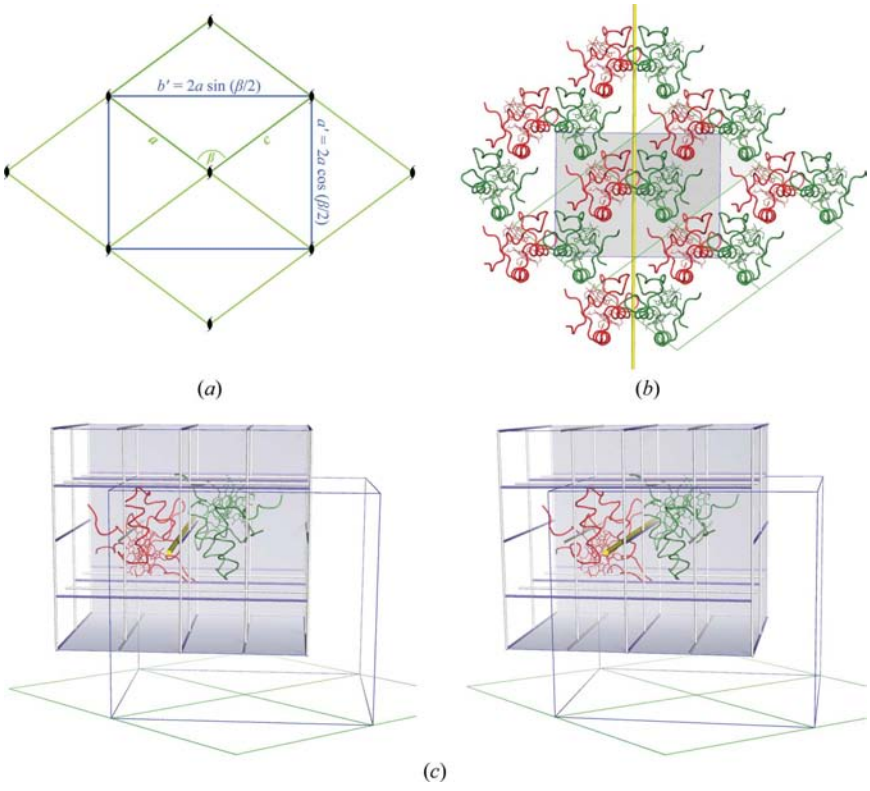

Figure 4
Noncrystallographic symmetry in DHC2 crystals. (*a*) A primitive monoclinic lattice with **a** ≃ **c** allows a C-centered orthorhombic setting with dimensions of $a' = 2a\cos(\beta/2)$, $b' = 2a\sin(\beta/2)$ and $c' = b$. The diagram shows a view of the **ac** (010) plane with the (unchanging) basis vector **b** pointing towards the viewer. (*b*) Crystal packing in a single layer of DHC2, showing the two molecules in the asymmetric unit of the $P2_1$ cell in red and green, respectively. The noncrystallographic symmetry axis connecting two monomers (yellow) almost satisfies a C-centred orthorhombic setup, albeit with an origin shift of $(\frac{1}{4}, \frac{1}{4}, \frac{1}{4})$. (*c*) Stereo representation of the $C222_1$ unit cell including ribbon representation of the DHC2 crystallographic dimer from space group $P2_1$ closely missing higher symmetry. Twofold rotation axes are shown in blue and twofold screw axes in white. The noncrystallographic twofold of the $P2_1$ cell (yellow) closely misses the axis of the higher symmetry cell.

obvious in the cumulative distribution of H, which shows nonlinear behaviour for all H in the case of DHC2 (Fig. 1*c*; Lebedev *et al.*, 2006). On the other hand, the normalized cumulative intensity distribution of Z differs less from untwinned data than would be expected for twinning with the apparent twin fraction α (Fig. 1*a*; Rees, 1980). This effect on the distribution of Z should be less pronounced in higher resolution shells, but the choice of resolution cutoff is crucial (Lebedev *et al.*, 2006) and in the case of DHC2 counteracts this effect, preventing clearer deviations beyond a resolution cutoff of 2.0 Å (data not shown).

3.4. Implications for crystal packing

It cannot be excluded that the occurrence of pseudo-merohedral twinning is related to different aspects of crystal growth and handling. The presence of NCS operations close to higher crystallographic symmetry may originate from the breaking of symmetry relations by physical transformation of the crystal parameters, for example in the processes of seeding, soaking, dehydration, cryocooling and data collection (Parsons, 2003; Lebedev *et al.*, 2006). In such cases, symmetry operations of the former higher crystal system can become distorted to noncrystallographic symmetry operations of a lower symmetry space group and turn into twinning operations. One possible way that this can occur is in crystals consisting of weakly interacting stacks of protein molecules with stronger interactions in two dimensions. Here, crystal contacts between the molecules in one plane are relatively strong, in contrast to weak interactions in the third dimension. If noncrystallographic symmetry is present in the layer plane, similar crystal contacts will connect the parallel layers on both layer sides. This increases the number of interactions, but it may also allow the presence of individual layers rotated around the noncrystallographic axis, resulting in a twinned crystal. This loose arrangement can be a result of sequential crystal growth, where binding energy and kinetics determine the twinning fraction α, and technically constitutes a statistical twin (Bragg & Howells, 1954; Cochran & Howells, 1954). Although the aspect of cell change through crystal manipulation does not seem to apply (no actual $C222_1$ crystal was observed in a large number of data collections), the crystal packing of DHC2 exemplifies this scheme: crystals are plate-like, indicating more efficient crystal packing in two dimensions compared with the third (Fig. 5). In the direction of **b**, crystal contacts are predominantly formed by the side chains of amino acids in poorly ordered loop regions (Fig. 6), providing only a weak basis for packing interactions in the third dimension. Owing to the noncrystallographic symmetry axis in the **ac** (010) plane, these loops face adjacent protein layers in both directions, exhibiting a very similar recognition pattern for molecular interactions of rotated protein layers. The tighter packing within layers of protein perpendicular to **b** is reflected in the area of the interaction surface between DHC2 monomers within and between layers. Each molecule has three closest neighbours within its layer (Fig. 5, opaque surfaces) and with these it shares interaction surfaces of 930.9, 1008.6 and 1121.5 Å^2, respectively. In contrast, all interactions between molecules in different layers along **b** have a significantly smaller interaction surface area of only 561.8 Å^2.

The packing features of DHC2 crystals can also be described using the OD (order/disorder) terminology introduced by Dornberger-Schiff (1956). It allows the classification of local disorder in crystals by considering the crystal to be composed of adjacent layers and their interactions (Dornberger-Schiff, 1956; Dornberger-Schiff & Grell-Niemann, 1961). If the subspace operations that relate individual crystal layers differ from the symmetry operations of the crystal's space group, the result is true disorder only if the local symmetry elements are not periodic. In cases where they do show periodicity, the lattice is ordered and can be fully described as an OD structure. The original OD terminology (Dornberger-Schiff, 1956) allows classification of local symmetry elements as either belonging to a first type, with parallel layer planes, or a second type, with rod structures of one-dimensional periodicity. Crystals of DHC2 can be classified as an OD structure of the first type, with layers in the **ac** plane building the crystal by translation along **b** (Fig. 6). These chemically homogeneous layers are not only related by translational symmetry, but are subject to local symmetry operations described by the twin law $l, -k, h$, generating a total of two different 'boundary layers' (Dornberger-Schiff & Grell-Niemann, 1961). DHC2 thus fulfils the conditions for an OD structure of type B, with identical layer compositions and a twinning operation that is isomorphous to the σ operation. As such, DHC2 represents an OD-twinned structure of type I/B (Nespolo *et al.*, 2004). This particular type of OD twinning seems to occur quite frequently and applies to various structures in the PDB [*e.g.* 1k7t

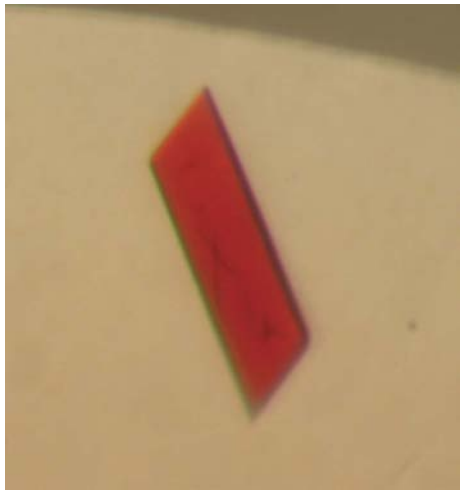

Figure 5
Macroscopic appearance of DHC2 crystals. The picture shows a crystal of DHC2 grown from 0.2 *M* $(NH_4)_2SO_4$, 32.5% PEG 4000, 0.1 *M* LiCl and 0.1 *M* citrate buffer pH 3.5. The direction with restrained growth is along **b**, perpendicular to the paper plane.

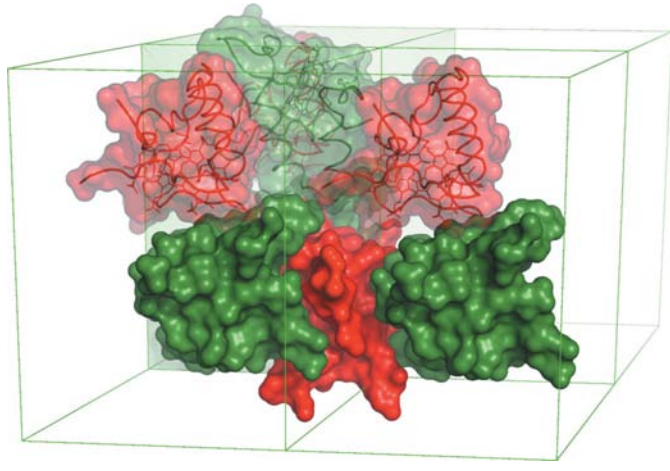

Figure 6
Crystal packing in DHC2. Crystal-packing interactions are significantly stronger in layers perpendicular to the **b** axis of the $P2_1$ cell than between these layers. This is reflected in an approximately doubled area of the interacting protein surfaces within the layers. All protein interactions between these layers are mediated by the same parts of the protein, allowing a rotation of the entire layer to create twinned domains and corresponds to the definition of an OD twin of family type I/B.

(Muraki *et al.*, 2002) and 2c8j] that were previously described as statistical twins (Bragg & Howells, 1954).

In addition to explaining the details of DHC2 crystal packing, this observation also suggests a possibility for a rational design approach. The loop regions involved in crystal-packing interactions could be altered by site-directed mutagenesis, with the aim of allowing stronger packing interactions in the direction of **b** and preferring the crystal symmetry interaction over the alternative local symmetry interaction leading to twinning. If suitable variants can be found this might abolish twinning, lead to a better three-dimensional growth behaviour and eventually to higher resolution data.

This work was supported by Deutsche Forschungsmgemeinschaft (grants Ei-520/2 and IRTG 1422). Diffraction data were collected on beamline BW7A at EMBL/DESY, Hamburg, Germany. The plasmid pEC86 was a kind gift from Professor Linda Thöny-Meyer (EMPA, St Gallen, Switzerland). The authors thank Markus G. Rudolph for stimulating discussions.

References

Adams, P. D., Grosse-Kunstleve, R. W., Hung, L.-W., Ioerger, T. R., McCoy, A. J., Moriarty, N. W., Read, R. J., Sacchettini, J. C., Sauter, N. K. & Terwilliger, T. C. (2002). *Acta Cryst.* D**58**, 1948–1954.
Arslan, E., Schulz, H., Zufferey, R., Kunzler, P. & Thöny-Meyer, L. (1998). *Biochem. Biophys. Res. Commun.* **251**, 744–747.
Barker, P. D. & Ferguson, S. J. (1999). *Structure*, **7**, 281–290.
Bragg, W. L. & Howells, E. R. (1954). *Acta Cryst.* **7**, 409–411.
Britton, D. (1972). *Acta Cryst.* A**28**, 296–297.
Brünger, A. T. (1993). *Acta Cryst.* D**49**, 24–36.
Brünger, A. T., Adams, P. D., Clore, G. M., DeLano, W. L., Gros, P., Grosse-Kunstleve, R. W., Jiang, J.-S., Kuszewski, J., Nilges, M., Pannu, N. S., Read, R. J., Rice, L. M., Simonson, T. & Warren, G. L. (1998). *Acta Cryst.* D**54**, 905–921.
Cochran, W. & Howells, E. R. (1954). *Acta Cryst.* **7**, 412–415.
Collaborative Computational Project, Number 4 (1994). *Acta Cryst.* D**50**, 760–763.
Dauter, Z. (2003). *Acta Cryst.* D**59**, 2004–2016.
Declercq, J.-P. & Evrard, C. (2001). *Acta Cryst.* D**57**, 1829–1835.
Dornberger-Schiff, K. (1956). *Acta Cryst.* **9**, 593–601.
Dornberger-Schiff, K. & Grell-Niemann, H. (1961). *Acta Cryst.* **14**, 167–177.
Einsle, O. (2001). In *Handbook of Metalloproteins*, edited by A. Messerschmidt, R. Huber, T. Poulos & K. Wieghardt. New York: Wiley.
Einsle, O., Messerschmidt, A., Stach, P., Bourenkov, G. P., Bartunik, H. D., Huber, R. & Kroneck, P. M. H. (1999). *Nature (London)*, **400**, 476–480.
Einsle, O., Stach, P., Messerschmidt, A., Simon, J., Kröger, A., Huber, R. & Kroneck, P. M. H. (2000). *J. Biol. Chem.* **275**, 39608–39616.
Emsley, P. & Cowtan, K. (2004). *Acta Cryst.* D**60**, 2126–2132.
Friedel, G. (1926). *Leçons de Cristallographie.* Nancy/Paris/Strasbourg: Berger Leurault.
Giacovazzo, C. (1992). *Fundamentals of Crystallography.* Oxford University Press.
Gouterman, M. (1978). *The Porphyrins*, Vol. III. New York: Academic Press.
Heitmann, D. & Einsle, O. (2005). *Biochemistry*, **44**, 12411–12419.
Herbst-Irmer, R. & Sheldrick, G. M. (1998). *Acta Cryst.* B**54**, 443–449.
Igarashi, N., Moriyama, H., Fujiwara, T., Fukumori, Y. & Tanaka, N. (1997). *Nature Struct. Biol.* **4**, 276–284.
Iverson, T. M., Arciero, D. M., Hsu, B. T., Logan, M. S. P., Hooper, A. B. & Rees, D. C. (1998). *Nature Struct. Biol.* **5**, 1005–1012.
Krissinel, E. & Henrick, K. (2004). *Acta Cryst.* D**60**, 2256–2268.
Larsen, N. A., Heine, A., de Prada, P., Redwan, E.-R., Yeates, T. O., Landry, D. W. & Wilson, I. A. (2002). *Acta Cryst.* D**58**, 2055–2059.
Laskowski, R. A., MacArthur, M. W., Moss, D. S. & Thornton, J. M. (1993). *J. Appl. Cryst.* **26**, 283–291.
Lebedev, A. A., Vagin, A. A. & Murshudov, G. N. (2006). *Acta Cryst.* D**62**, 83–95.
Liang, J., Ealick, S., Nielsen, C., Schreiber, S. L. & Clardy, J. (1996). *Acta Cryst.* D**52**, 207–210.
Matthews, B. W. (1968). *J. Mol. Biol.* **33**, 491–497.
Muraki, M., Ishimura, M. & Harata, K. (2002). *Biochim. Biophys. Acta*, **1569**, 10–20.
Murshudov, G. N., Vagin, A. A. & Dodson, E. J. (1997). *Acta Cryst.* D**53**, 240–255.
Nespolo, M., Ferraris, G., Durovic, S. & Takeuchi, Y. (2004). *Z. Kristallogr.* **219**, 773–778.
Otwinowski, Z. & Minor, W. (1997). *Methods Enzymol.* **276**, 307–326.
Padilla, J. E. & Yeates, T. O. (2003). *Acta Cryst.* D**59**, 1124–1130.
Parsons, S. (2003). *Acta Cryst.* D**59**, 1995–2003.
Rees, D. C. (1980). *Acta Cryst.* A**36**, 578–581.
Rudolph, M. G., Wingren, C., Crowley, M. P., Chien, Y. & Wilson, I. A. (2004). *Acta Cryst.* D**60**, 656–664.
Sheldrick, G. M. (2002). *Z. Kristallogr.* **217**, 644–650.
Sheldrick, G. M. (2008). *Acta Cryst.* A**64**, 112–122.
Stevens, J., Daltrop, O., Allen, J. & Ferguson, S. (2004). *Acc. Chem. Res.* **37**, 999–1007.
Sultana, A., Alexeev, I., Kursula, I., Mäntsälä, P., Niemi, J. & Schneider, G. (2007). *Acta Cryst.* D**63**, 149–159.
Thöny-Meyer, L. (1997). *Microbiol. Mol. Biol. Rev.* **61**, 337–376.
Tong, L. & Rossmann, M. G. (1990). *Acta Cryst.* A**46**, 783–792.
Weiss, M. S. (2001). *J. Appl. Cryst.* **34**, 130–135.
Weiss, M. S. & Hilgenfeld, R. (1997). *J. Appl. Cryst.* **30**, 203–205.
Wittmann, J. G. & Rudolph, M. G. (2007). *Acta Cryst.* D**63**, 744–749.
Yang, F., Dauter, Z. & Wlodawer, A. (2000). *Acta Cryst.* D**56**, 959–964.
Yeates, T. O. (1997). *Methods Enzymol.* **276**, 344–358.
Yeates, T. O. & Fam, B. C. (1999). *Structure Fold. Des.* **7**, R25–R29.